RSC Advances

ROYAL SOCIETY OF CHEMISTRY

www.rsc.org/advances

RSC Advances

RSCPublishing

PAPER

Electronic transport behaviours of lead chalcogenides $(PbE)_n$ (E=S and Se) nanocluster junctions by *ab–initio* simulation

Cite this: DOI: 10.1039/xoxxoooooox

Received ooth January 2012,
Accepted ooth January 2012

DOI: 10.1039/xoxxoooooox

www.rsc.org/

Rong LI,[a] Jianbing ZHANG,[a, b] Yuanlan XU,[a] Xiangshui MIAO [a,b] and Daoli ZHANG[a, b, *]

Lead chalcogenide nanoclusters possess relatively narrow band gaps and large Bohr exciton radii, making them indispensable in many modern applications. All the potential applications require the integration of their nanoclusters into the scalable and robust device structures In this paper, the geometric structural behaviour of the nanoscale lead chalcogenides $(PbS)_n$ and $(PbSe)_n$ (n=2, 3, 4) clusters as well as their electronic transport properties are comparatively investigated by employing *ab–initio* simulation of non–equilibrium Green's function (NEGF) combined with density functional theory (DFT). Results indicate that all the investigated $(PbS)_n$ and $(PbSe)_n$ nanocluster–based molecular junctions show metallic behavior at low biases ([–2V, 2V]) while negative differential resistance (NDR) appears at a certain high bias range. Our calculation shows that the current of $(PbE)_3$ nanocluster–based molecular junction is almost the smallest at any bias. The mechanisms of the current–voltage characteristics of all the $(PbE)_n$(E=S and Se) nanocluster junctions are proposed.

I. INTRODUCTION

In recent years, numerous theoretical investigations have been reported on the electronic transport properties of molecular devices. It is believed that molecular devices will take the place of microelectronic devices in future by the virtue of small size, low energy consumption and low cost. Many interesting physical properties have been found in these devices, such as negative differential resistance (NDR)[1], electrical switching[2], single–electron characteristics[3], Coulomb blockade[4], current rectification[5], and so on. However, most of the molecular devices reported to date are based on small organic molecules[6, 7], C_{60}[1, 8], graphite[9, 10] or these materials with some modifications[2, 11, 12]. Very few works have attempted to study the transport properties of junctions based on inorganic clusters, such as lead chalcogenides, GaAs, InAs, et al.

Lead chalcogenides, designated as PbS, and PbSe in this work, have recently been the subject of extensive theoretical and experimental research owing to their unique behavior. Notably, they possess relatively narrow band gaps (direct gaps at L point of 0.29 eV, and 0.27 eV for PbS, and PbSe respectively) , which crystallize at ambient condition in the cubic rock–salt structure, and possess 10 valence electrons instead of eight for common zinc–blend and wurtzite III–V and II–VI compounds. These narrow–gap PbS and PbSe semiconductors exhibit some unusual electronic and structural properties, such as very narrow energy gaps, anomalous order of band gaps and valence–band maximum energies versus anion atoms, negative (positive) band–gap pressure (temperature) coefficient, high carrier mobility, and high dielectric constant. All these factors have contributed toward the great interest in the fundamental study of this group of semiconductors, which make them potentials candidates for different technological applications. In particular, they have been used for optoelectronic[13], ferroelectricity[14], or spintronic devices [15], especially in long wavelength imaging [16], infrared laser diodes[17] and for thermophotovoltaic energy converters [18]. Understanding the electronic structure and transport properties of PbE is important for all of these properties and applications. In the field of theoretical study, Koirala et al.[19] studied the geometric and electronic structures of both neutral and negatively charged lead sulfide clusters, for n=2–10. The theoretical researches on PbSe nanoscale materials are mainly about the multiple exciton generation or carrier multiplication of PbSe nanocrystals[20]. Fischer et al. [21] investigated the structures and excited states of neutral and positively charged $(PbSe)_4$ clusters. Peng et al. [22] reported the electronic structure and transport properties of doped bulk PbSe semiconductor.

Although considerable progress has been made concerning theoretical description of the structural and electronic

properties of lead chalcogenides compounds, there is a real lack of knowledge of electronic transport properties of their nanoclusters. Up to present, there is little coverage of theoretical reports on the transport properties of lead chalcogenides nanocluster–based molecular devices in the literature.

All the potential applications of lead chalcogenides require the integration of their nanoclusters into scalable and robust device structures. In this work, we investigate the electronic transport properties of lead chalcogenides [$(PbE)_n$ (E=S and Se; n=2–4)] nanocluster molecular junctions. Interestingly, the inorganic $(PbE)_n$ nanocluster–based molecular junctions studied here also display some properties obtained in organic molecular devices. The present findings could open a door to the integration of inorganic nanoscale devices in the field of nanoelectronics.

II. GEOMETRIC STRUCTURE AND COMPUTATIONAL METHOD

The structures of $(PbS)_n$ and $(PbSe)_n$ (n=2–4) nanoclusters are optimized and showed in Figures 1(a) and 1(b), The geometric configuration of $(PbS)_2$ is bent rhombi with a dihedral angle (S–Pb–Pb–S) of 148.4º. The geometry of $(PbS)_3$ and $(PbSe)_3$ is a trigonal bipyramid with a third coplaner S or Se atom. The optimized structure of $(PbS)_4$ and $(PbSe)_4$ is a perfect cube with a Pb–S bond length of 2.66Å and Pb–Se bond length of 2.84 Å, respectively, which agree well with previous study[19]. The geometric configuration of $(PbSe)_2$ is rhombi with Pb–Se bond length of 2.67 Å.

All the other geometric configuration parameters of $(PbS)_n$ and $(PbSe)_n$ nanoclusters are shown in Figure 1 with reasonable differences from the reference due to different calculation methods.

The quantum transport properties in the $(PbE)_n$ (n=2–4) nanocluster junctions are calculated by employing *ab initio* simulation. The configurations studied here are illustrated in Figures 2, which are divided into three regions: the left electrode, the central scattering region and the right electrode. The scattering region includes the $(PbE)_n$ nanoclusters and a portion of the semi–infinite electrodes to screen the interaction between $(PbE)_n$ nanoclusters and the electrodes. The extended region consists of molecule with 2×2 (001) two layers of Au slab in the left electrode as well as two layers in the right electrode. The $(PbE)_n$ nanoclusters are so small that a 2×2 layers in x and y directions is large enough. However, eight layers[23] of Au slab were chosen in z direction and then they decrease to five layers[24] in some current studies for a fast computational speed. In this present work, only four layers of Au slab are used because they are enough for such small clusters. The perpendicular distance between the left electrode and the leftmost atom of the cluster as well as counterpart in the right is 2.0 Å, which is a typical distance in the interface between the electrode and molecules[25]. We keep all gold atoms fixed and relax the clusters in the centre until the force on each atom is smaller than 0.05 eV/Å in the optimization.

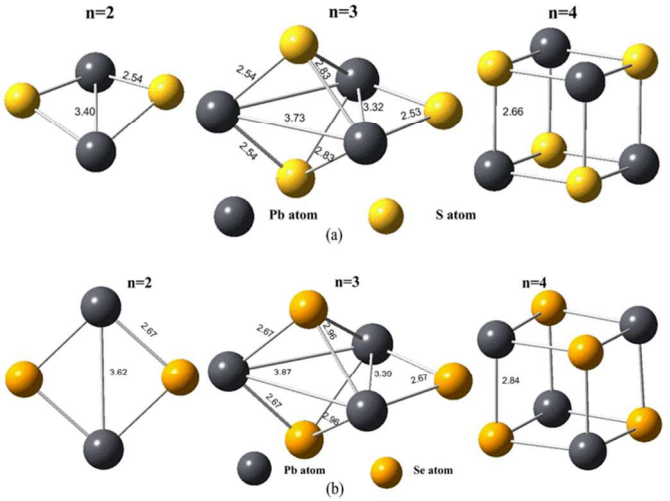

Figure 1. Structures of optimized $(PbE)_n$ (n=2–4) nanoclusters. Bond lengths take Å as the unit. (a) $(PbS)_n$, and (b) $(PbSe)_n$.

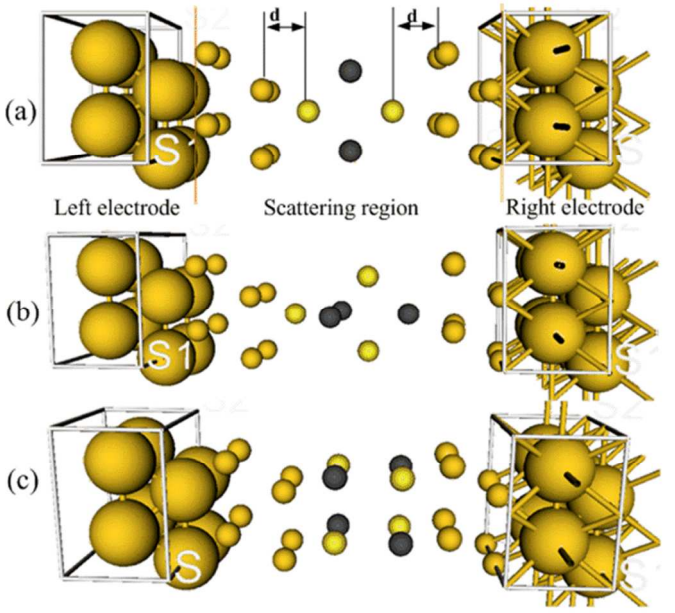

Figure 2. Schematic plot of $(PbE)_n$ molecular junction for: (a) n=2, (b) n=3 and (c) n=4. The junction consists of three regions. The extended region consists of molecule 2×2 (001) two layers of Au slab in the left electrode and two layers of Au slab in the right electrode, between which is the scattering region. d is the left and right axial distance.

In our simulations, Perdew–Burke–Ernzerhof version of the generalized gradient approximation (GGA.PBE) is employed.[26, 27] The electron wave function (or Mulliken population or the valence electrons) are expanded in a single–ξ along with polarization basis set (SZP) for Au atoms and a double–ξ along with polarization basis set (DZP) for other atoms.

The Brillouin zone is set to be 5×5×100 points following the Monkhorst–Pack k–point scheme. The cut–

off energy and the iterated convergence criterion for total energy are set to 150 Rydberg and 10^{-5} respectively.

III. RESULTS AND DISCUSSION

The current-voltage (*I–V*) curves of $(PbS)_n$ and $(PbSe)_n$ (n = 2–4) nanocluster–based molecular junctions were calculated as the bias voltages vary from –3.0 V to 3.0 V in steps of 0.2 V, as shown in Figure 3. It is noted that the current is obtained self–consistently under non–equilibrium conditions at each bias voltage. In NEGF theory, the *I–V* characteristics are determined by the Landauer–Bütiker formula[28]:

$$I(V)=\frac{2e}{h}\int_{\mu_L}^{\mu_R}[f(E-\mu_L)-f(E-\mu_R)]T(E,V)dE \quad (1)$$

where *e* is the electron charge, *f* the Fermi function, *h* Planck's constant, *T(E,V)* the transmission function of the system, and μ_R as well as μ_L the electrochemical potential of the right and left electrodes, respectively. $\mu_R=E_F-eV/2$ and $\mu_L=E_F+eV/2$. The Fermi level of the system E_F is set to be zero in all the calculations. The transmission function *T(E,V)* of the system is the sum of the transmission probabilities of all channels available at energy *E* under the bias voltage *V*[28],

$$T(E,V)=T_r\left[\Gamma_L(V)G^R(E,V)\Gamma_R(V)G^A(E,V)\right] \quad (2)$$

where coupling functions Γ_L and Γ_R are the imaginary parts of the left and right self–energies, G^R and G^A are the retarded and advanced Green's functions, respectively.

From Figures 3, it could obviously be observed that all $(PbE)_n$ (n=2–4) nanocluster–based junctions show the metal characteristics, with a linear region from –2.0 V to 2.0 V. This is due to the interaction between the nanoclusters and the metal electrodes, resulting from the electrons of Au electrodes doping into $(PbE)_n$ nanoclusters. As illustrated in Figure 4, the total valence electrons (Mulliken population) of $(PbE)_n$ (n=2–4) is more than 20, 30, and 40 respectively at any bias voltages except a few points at high bias voltages. When the bias voltage increases to some point, the currents of all the six systems decrease gradually and then NDR appears almost symmetrically on both the positive and negative bias ranges.

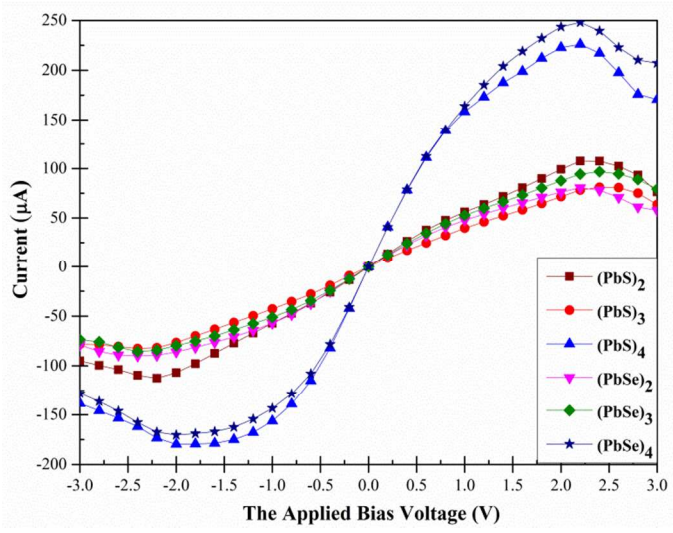

Figure 3. The current–voltage characteristics for $(PbE)_n$ nanocluster–based junctions, in which E=S and Se, and n=2,3 and 4 respectively.

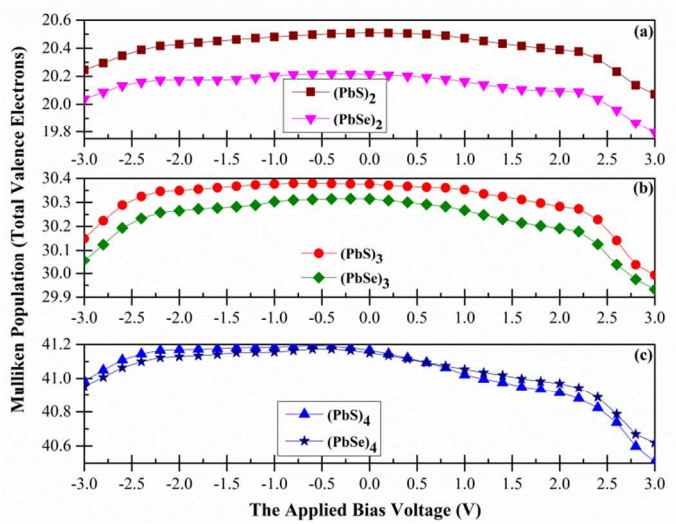

Figure 4. Mulliken population (the total valence electrons) of $(PbE)_n$ nanoclusters at the different applied bias voltages. (a) $(PbE)_2$, (b) $(PbE)_3$ and (c) $(PbE)_4$.

Figures 4 also provides evidence for this NDR feature. It can be found that the electrons doped from Au electrodes into the $(PbE)_n$ nanoclusters decreases rapidly when the bias voltage is out of the range from –2 V to2 V, giving directly rise to the decrease of the current.

In Figure 3, the absolute currents of $(PbE)_4$ clusters are largest. For $(PbS)_4$ clusters, they are 179.6 μA at –2.0 V and 226.1 μA at 2.2 V for respectively and then decrease to 138.5 μA at –3.0 V and 170.7 μA at 3.0 V respectively. The average decreasing speeds on positive and negative region are 69.2 μA/V and 41.1 μA/V, respectively; while for $(PbSe)_4$ clusters, they are 170.4 μA at –2.0 V and 240.8 μA at 2.2 V for respectively and then decrease to 128.3 μA at –3.0 V and 207.1 μA at 3.0 V respectively. The average decreasing speeds on positive and negative region are 51.1 μA/V and 42.1 μA/V, respectively. This more obvious NDR feature on positive side is due to the much more rapid decrease of Mulliken population of $(PbE)_4$ shown in Figure 4. It is known that the asymmetric structures of nanoclusters will lead to the asymmetric *I–V* curves. From Figure 3, it can be found that the *I–V* curve of $(PbE)_4$ is not completely symmetric at both positive and negative bias region. In practice, $(PbE)_4$ nanoclusters do not have the perfect symmetric structures. The ground state geometry of lead chalcogenide tetramers is a cube with alternating Pb and S (or Se) atoms. This is the smallest lead chalcogenide clusters, whose stabilization is governed by Pb–S (or Pb–Se) bonds. Our calculation indicates that $(PbE)_4$ nanoclusters is a distorted cube, with two distinct Pb–S–Pb (or Pb–Se–Pb) and S–Pb–S (or Se–Pb–Se) bond angles, respectivel. Two Pb–S–Pb bond angles are 89.8º and 90.4º, and two S–Pb–S bond angles 89.6º and 90.2º, Two Pb–Se–Pb bond angles are 89.9º and 90.2º, and two Se–Pb–Se bond angles 89.7º and 90.3º. All of them deviate from

90º in the perfect cube. In addition, due to the different electronegativity between Pb and S (or Se) atoms, there are the unequal interaction forces between Au atoms and Pb and S (or Se) atoms. As a result, the contacts of $(PbE)_n$ nanoclusters with the right and left electrodes are not completely symmetrical. Moreover, although the quantum current varies for different PbE nanoclusters at any given bias voltage, the current of $(PbE)_4$–based nanocluster junction is almost the largest at any bias voltage, as shown in Figure 3. This can also be explained by Figure 4 that more electrons are doped into $(PbE)_4$ than $(PbE)_2$ or $(PbE)_3$ from Au electrodes.

From Figure 4, we can also observe that the number of electrons decreases more rapidly on positive bias range than on negative bias range, which results in more obvious NDR feature on positive bias range as shown Figure 3.

In order to gain a deeper understanding of the electronic transport properties of the different nanocluster junctions shown in Figure 3, we further calculated the transmission coefficient *T(E,V)* and density of states (DOS) of $(PbE)_n$ nanoclusters in the energy range from –2.0 eV to + 2.0 eV at zero bias voltages as illustrated in Figure 5. According to Equation (2), the current through a molecular junction depends on the transmission amplitude within the bias window of $[\mu_R(V), \mu_L(V)]$. Since the Fermi level is set to be zero in our calculations, the actual region of the bias window is $[-V/2, V/2]$. All molecular orbitals around the Fermi level can contribute to the electronic transport, especially at the low bias voltages. If an orbital delocalizes across the molecule, an electron that reaches the molecule at the energy of this delocalized orbital has a high mobility. Hence, it corresponds to a certain peak in the transmission spectra *T(E)*.

From the transmission spectra *T(E,V=0)* shown in Figures 5 and 6, it can be observed that the number of molecular orbitals contributing to the electronic transport near the Fermi level is $(PbS)_3$>$(PbS)_2$>$(PbS)_4$ and $(PbSe)_3$>$(PbSe)_2$> $(PbSe)_4$ respectively. In contrast, the transmission amplitudes of $(PbE)_4$ near the Fermi level are much larger than those of $(PbE)_2$ or $(PbE)_3$. Under the joint action of these two opposite

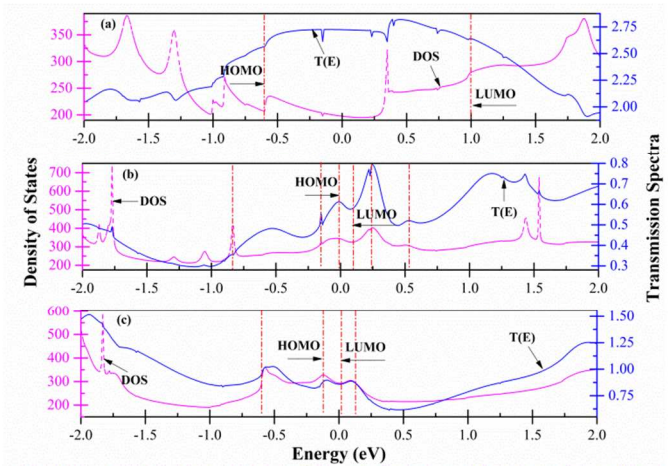

Figure 5. The transmission spectra and the DOS of $(PbS)_n$ at zero bias voltage. The transmission spectra are in blue while the DOS in red. The dotted lines indicate the molecular orbitals and the Fermi level E_F is zero with automatic setting. (a) $(PbS)_4$, (b) $(PbS)_3$ and (c) $(PbS)_2$

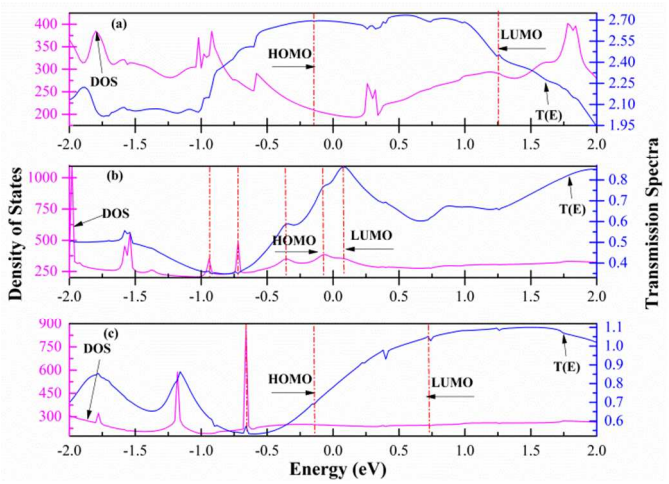

Figure 6. The transmission spectra and the DOS of $(PbSe)_n$ at zero bias voltage. The transmission spectra are in blue while the DOS in red. The dotted lines indicate the molecular orbitals and the Fermi level EF is zero with automatic setting. (a) $(PbSe)_4$, (b) $(PbSe)_3$ and (c) $(PbSe)_2$

factors, the currents of $(PbS)_4$ and $(PbSe)_4$ are the largest as shown in Figure 3, providing the evidence that the transmission amplitude plays a more important role in determining the current of $(PbE)_n$ nanocluster junctions. In fact, The transmission amplitude depends on the energy of the delocalized orbital and the applied bias voltage.There is a good match between the peaks of transmission spectra and those of the DOS. It can be seen clearly in Figure 5 that the molecular energies beside the highest occupied molecular orbital (HOMO) and the lowest unoccupied molecular orbital (LUMO) match well between the peaks of transmission coefficient and those of the DOS.

In order to know more about the NDR behaviour of the molecular junctions, the transmission spectra and density of states of $(PbS)_2$ and $(PbSe)_2$ at the various bias voltages as a function of energy level are calculated and plotted in Figures

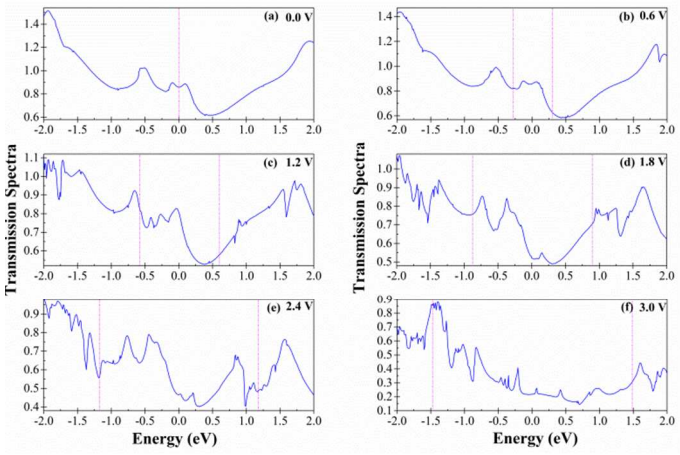

Figure 7. The transmission spectra of $(PbS)_2$ system at the various applied bias voltages. The Fermi level E_F is set to be the origin of energy and the regions between the two vertical dash lines refer to the bias window. (a) the bias voltage =0.0 V, (b) the bias voltage =0.6 V, (c) the bias voltage =1.2 V, (d) the bias voltage =1.8 V, (e) the bias voltage = 2.4 V, and (f) the bias voltage = 3.0 V.

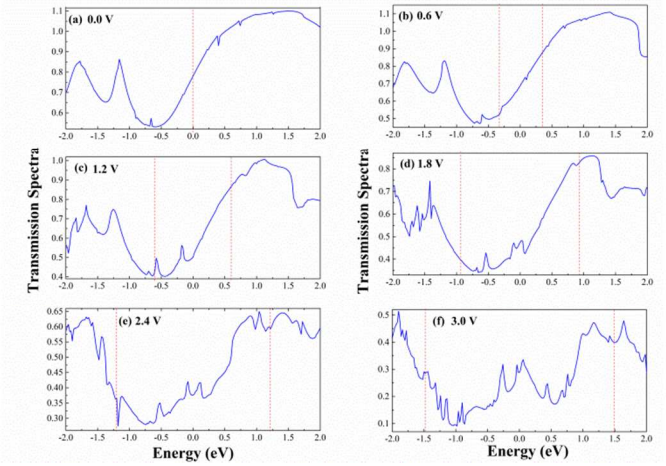

Figure 8. The transmission spectra of $(PbSe)_2$ system at the various applied bias voltages. The Fermi level E_F is set to be the origin of energy and the regions between the two vertical dash lines refer to the bias window. (a) the bias voltage =0.0 V, (b) the bias voltage =0.6 V, (c) the bias voltage =1.2 V, (d) the bias voltage =1.8 V, (e) the bias voltage = 2.4 V, and (f) the bias voltage = 3.0 V.

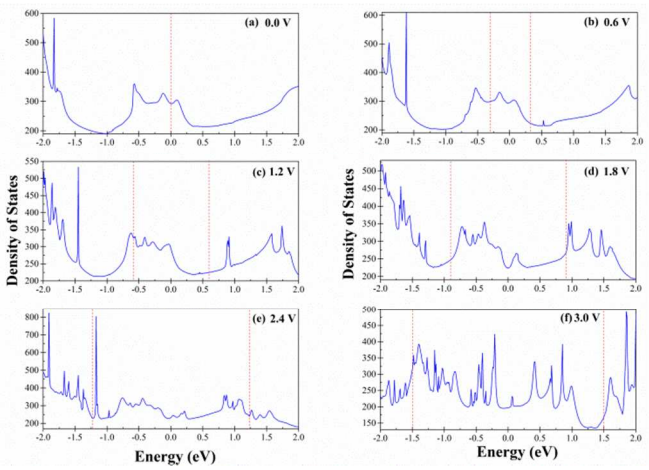

Figure 9. The density of states of $(PbS)_2$ system at the various applied bias voltages. The Fermi level E_F is set to be the origin of energy and the region between the two vertical dash lines refer to the bias window. (a) the bias voltage =0.0 V, (b) the bias voltage =0.6 V, (c) the bias voltage =1.2 V, (d) the bias voltage =1.8 V, (e) the bias voltage = 2.4 V, and (f) the bias voltage = 3.0 V.

7, 8, 9, and 10, respectively. The regions between the two vertical dash lines stand for the bias window. From Figures 7 and 8, it can be seen that more and more transmission peaks enter into the bias window and contribute to the transport current $(PbE)_2$ nanocluster junctions with the increase of the applied bias voltage, which leads to an approximately linear increase in the current and shows the metallic behaviour of the devices at the low bias voltages. However, as the external bias voltages increase further, the amplitudes of transmission coefficients decrease rapidly at the same time.

As a result, the total current of the device decreases and NDR appears at the large bias voltage, as shown in Figure 3. The DOS of $(PbS)_2$ and $(PbSe)_2$ (as shown in Figures 9 and 10) can also explain this phenomenon. More DOS peaks enter into the bias window with the increase of the applied bias voltages. However, when the bias voltage rises to 2.4 V, the peaks are narrowed obviously, which causes negative effect to the current of the devices.

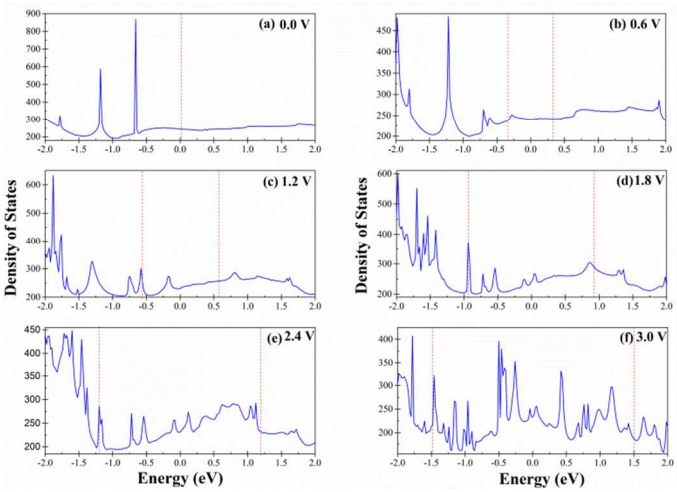

Figure 10. The density of states of $(PbSe)_2$ system at the various applied bias voltages. The Fermi level E_F is set to be the origin of energy and the region between the two vertical dash lines refer to the bias window. (a) the bias voltage =0.0 V, (b) the bias voltage =0.6 V, (c) the bias voltage =1.2 V, (d) the bias voltage =1.8 V, (e) the bias voltage = 2.4 V, and (f) the bias voltage = 3.0 V.

Conclusions

In conclusion, we have investigated the electronic transport properties of $(PbE)_n$ (E= S and Se, n=2–4) nanocluster–based molecular junctions employing a combined DFT with NEGF approach. By computing the *I–V* curves of these molecular junctions, it has been shown that all the investigated six molecular junctions appear metallic transport behavior at low biases and then give rise to NDR behavior beyond certain high biases, which is found to be related to the number of electrons doped into $(PbE)_n$ nanoclusters from electrode Au atoms. The current of $(PbS)_4$–based molecular junction is the largest while that of $(PbS)_3$–based molecular junction is the smallest at any bias voltage. The order of the current value is $(PbSe)_4 > (PbSe)_3 > (PbSe)_2$ while the difference between $(PbSe)_2$ and $(PbSe)_3$ is very small. The characteristics of the *I–V* curves are ascribed to the combination effects of the transmission peaks entering into the bias window and the transmission amplitude but the later factor plays a more important part. Compared to $(PbS)_2$ or $(PbS)_3$, $(PbS)_4$ based molecular device is more suitable for the future application because of its large current and obvious NDR feature.

Acknowledgements

This work was supported by the National Natural Science Foundation of China (NSFC No. 51302096), the Fundamental Research Funds of Wuhan City (No. 2013060501010163), the

Fundamental Research Funds of Huazhong University of Science and Technology (No. 2011QN003) and the Graduate Innovation Fund of Huazhong University of Science and Technology (No. HF–11–09–2013). The authors thank Chen Xia and the Analytical and Testing Centre of Huazhong University of Science and Technology for the help on computing.

Notes and references

[a] School of Optical and Electronic Information, Huazhong University of Science and Technology, No. 1037 Luoyu Road, Hongshan District, Wuhan City, Hubei Province, 430074, P. R. China. Electronic mail: zhang_daoli@ hust.edu.cn
[b] Wuhan National Laboratory for Optoelectronics, 1037 Luoyu Road, Hongshan District, Wuhan City, Hubei Province, 430074, P. R. China

1 X J Zhang, M Q Long, K Q Chen, Z Shuai, Q Wan, B S Zou, and Y Zhang, Electronic transport properties in doped C60 molecular devices. *Applied Physics Letters*, **94**(7): 073503(3)(2009).
2 M Qiu, Z H Zhang, X Q Deng, and K Q Chen, Conduction switching behaviors of a small molecular device, *Journal of Applied Physics*, **107**(6): 063704(5) (2010).
3 R P. Andres, T Bein, M Dorogi, S Feng, J I Henderson, C P Kubiak, W Mahoney, R G Osifchin, R Reifenberger, "Coulomb Staircase" at Room Temperature in a Self–Assembled Molecular Nanostructure. *Science*, **272**(5266): 1323–1325(1996).
4 J J Palacios, Coulomb blockade in electron transport through a C60 molecule from first principles. *Physical Review B*, **72**(12): 125424(6)(2005).
5 J B Pan, Z H Zhang, K H Ding, X Q Deng, and C Guo, Current rectification induced by asymmetrical electrode materials in a molecular device. *Applied Physics Letters*, **98**(9): 092102(3)(2011).
6 Q L Bao, Z S Lu, J Li, K P Loh, and C M Li, Theoretical and Experimental Studies of Electronic Transport of Dithienothiophene. *The Journal of Physical Chemistry C*, **113**(28): 12530–12537(2009).
7 X Q Deng, J C Zhou, Z H Zhang, G P Tang, and M Qiu, Electrode metal dependence of the rectifying performance for molecular devices: A density functional study. *Applied Physics Letters*, **95**(10): 103113(3)(2009).
8 Z Q Fan, and K Q Chen, Controllable rectifying performance in a C60 molecular device with asymmetric electrodes. *Journal of Applied Physics*, **109**(12): 124505(4)(2011).
9 J He, K Q Chen, Z Q Fan, L M Tang, and W P Hu, Transition from insulator to metal induced by hybridized connection of graphene and boron nitride nanoribbons. *Applied Physics Letters*, **97**(19): 193305(3)(2010).
10 X J Zhang, K Q Chen, L M Tang, M Q Long, Electronic transport properties on V–shaped–notched zigzag graphene nanoribbons junctions. *Physics Letters A*, **375**(37): 3319–3324(2011).
11 P Zhao, D S Liu, First–principles study of the electronic transport properties of a C131 –based molecular junction. *Solid State Communications*, **151**(20): 1424–1427(2011).
12 H Ren, Q X Li, Q W Shi, and J L Yang, *Quantum Dot Based on Z–shaped Graphene Nanoribbon: First–principles Study*. Chinese Journal of Chemical Physics, **20**(4): 489–494(2007).
13 A I Lebedev, and I A Sluchinskaya, Ferroelectric phase transitions in IV–VI semiconductors associated with off–center ions, *Ferroelectrics*, **157**(1), 275–280(1994).
14 B Akimov, A Dmitriev, D Khohlov, and L Ryabova, Carrier Transport and Non–Equilibrium Phenomena in Doped PbTe and Related Materials, *Phys. Status Solidi A*, **137**(1), 9–55 (1993).
15 S Jin, H Wu, and T Xu, Large Rashba splitting in highly asymmetric CdTe/PbTe/PbSrTe quantum well structures, *Appl. Phys. Lett.*, **95**(13), 132105(3) (2009).
16 K. Hummer, A. Gruneis, G. Kresse, Structural and electronic properties of lead chalcogenides from first principles, *Phys. Rev. B*, **75**(19), 195211(9) (2007).
17 H Preir, Recent advances in lead–chalcogenide diode lasers, *Appl. Phys*. **20**(3), 189–206(1979).
18 H Zogg, A Fach, J John, J Mosek, P Muller, C Paglino, W Buttler, Photovoltaic lead–chalcogenide on silicon infrared sensor arrays, *Opt. Eng*. **33**(5), 1440–1449(1994).
19 P Koirala, B Kiran, A K Kandalam, C A Fancher, H L de Clercq, X Li, and K H Bowen, Structural evolution and stabilities of neutral and anionic clusters of lead sulfide: Joint anion photoelectron and computational studies. *The Journal of Chemical Physics*, **135**(13): 134311(12)(2011).
20 C M Isborn, and O V Prezhdo, Charging Quenches Multiple Exciton Generation in Semiconductor Nanocrystals: First–Principles Calculations on Small PbSe Clusters. *The Journal of Physical Chemistry C*, **113**(29): 12617–12621(2009).
21 S A Fischer, C M Isborn, and O V. Prezhdo, Excited states and optical absorption of small semiconducting clusters: Dopants, defects and charging. *Chemical Science*, **2**(3): 400–406(2011).
22 H W Peng, J H Song, M G Kanatzidis, and A J Freeman, Electronic structure and transport properties of doped PbSe, *Physical Review B*,. **84**(12): 125207(13)(2011).
23 Z. X Dai, X Q Shi, X H Zheng, X L Wang and Z Zeng, *Ab initio* investigations of the transport properties of a Ge7 cluster, *Physical Review B*, **75** (15), 155402(8) (2007).
24 G Ji, Y Zhai, C Fang, Y Xu, B Cui, and D Liu, The electronic transport properties in C60 molecular devices with different contact distances, *Physics Letters A*, **375** (14), 1602–1607 (2011).
25 H Sellers, A Ulman, Y Shnidman, and J E Eilers, Structure and binding of alkanethiolates on gold and silver surfaces: implications for self–assembled monolayers, *Journal of the American Chemical Society,* **115** (21), 9389–9401 (1993).
26 J P Perdew, K Burke, and M Ernzerhof, Generalized Gradient Approximation Made Simple. *Physical Review Letters*, **77**(18): 3865–3868(1996).
27 Y H Zhou, J B Zhang, D L Zhang, C Ye, and X S Miao, Phosphorus-doping-induced rectifying behavior in armchair graphene nanoribbons devices. *Journal of Applied Physics*, **115**(1): 013705 (2014)
28 Y H Zhou, D L Zhang, J B Zhang, C Ye, and X S Miao, Negative differential resistance behavior in phosphorus-doped armchair graphene nanoribbon junctions. *Journal of Applied Physics*, **115**(7):073703 (2014)
29 S Datta, *Electronic transport in mesoscopic systems*, Cambridge University Press,1995

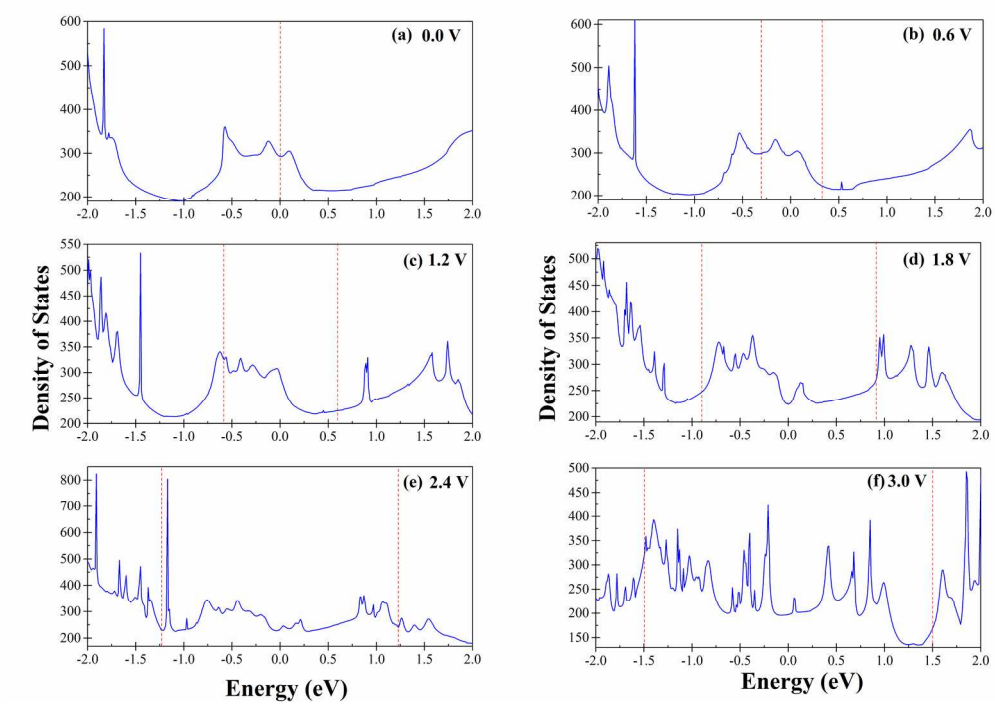

The density of states of (PbS)2 system at the various applied bias voltages. The Fermi level EF is set to be the origin of energy and the region between the two vertical dash lines refer to the bias window. (a) the bias voltage =0.0 V, (b) the bias voltage =0.6 V, (c) the bias voltage =1.2 V, (d) the bias voltage =1.8 V, (e) the bias voltage = 2.4 V, and (f) the bias voltage = 3.0 V.
201x141mm (300 x 300 DPI)